Departamento de Biología Celular
Universidad de Barcelona

Sexual reproduction in demosponges: ecological and evolutive implications

Reproducción sexual en demosponjas: implicaciones ecológicas y evolutivas

Ana Riesgo Gil

Barcelona 2007

Chapter 2:

Introduction

The Porifera (sponges) are simple invertebrates. They are widely regarded as the most basal phylum of animals, but their phylogenetic relationships with both other diploblasts and basal triploblasts remain controversial (e.g., Maldonado 2004; Wang and Lavrov 2007). The Porifera are classified into three taxonomic classes: Hexactinellida, Calcarea, and Demospongiae. The latter class is comprised of approximately 6000 valid species, and is about 85% of the known Porifera (Hooper and van Soest 2002); it is also the most studied and, consequently, the best understood group.

Body architecture is relatively uniform across Demospongiae. The body is typically permeated by numerous aquiferous canals, through which the ambient water flows in and out transporting particulate food, oxygen, and excretes. There is an external epithelium of flattened cells (exopinacocytes) and an internal epithelium of similar pseudoepithelial flattened cells (endopinacocytes) lining the walls of the aquiferous canals. Chamber-like expansions of the canals are lined by flagellated collar cells (choanocytes) that capture bacteria and occasionally microplankton. A collagen-rich inter-epithelial mesenchyme, the mesohyl, harbours diverse populations of amoeboid cells, the mineral and/or the organic skeletal elements, and usually a collection of prokaryotic and/or eukaryotic endosymbionts (e.g., Brien 1973; Simpson 1984).

The relative uniformity in cell composition and body architecture across Demospongiae (e.g., Brien 1973; Simpson 1984) strongly contrasts with the diversity in

sexual reproduction known in this class. The available data indicate that embryonic development may proceed in Porifera through at least 6 different gastrulation modes (Leys 2004; Maldonado 2004), 3 of which occur in the class Demospongiae (i.e., centrifugal migration, selective centrifugal migration, and emboly). Likewise, 6 different morphological larval types have been described in Demospongiae to date, namely cinctogastrula (formerly cinctoblastula), hoplitomella, clavablastula, tufted parenchymella, non-tufted parenchymella, and dispherula, and new types are predicted to be described in the future since the larva of many sponge families continue to be identified (reviewed by Maldonado and Bergquist 2002; Maldonado 2006). Further, some demosponge groups lack the larval stage, experiencing direct development (e.g., Watanabe and Masuda 1990; Sarà et al. 2002).

The absence of gonads and a distinct germ cell line is a feature common to all sponges. At the time of reproduction, some somatic cells, either choanocytes or totipotent archaeocytes, become gonial cells and produce gametes. Again, gametogenesis unfolds as a quite variable process, with cases of gonochorism, successive hermaphroditism, and contemporaneous hermaphroditism, depending on the taxon (i.e., Fell 1983; Reiswig 1983; Boury-Esnault and Jamieson 1999). The phylogenetic significance of the diversity that affects the process of sexual reproduction remains unclear because the underlying ecological, physiological, and/or biological pressures are poorly understood.

Despite the variability affecting most aspects of sexual reproduction in sponges, there are recognizable patterns in reproductive timing, which is regulated mostly by environmental factors, such as temperature, photoperiod, or lunar cycles (e.g., Reiswig 1970, 1983; Fell, 1974, 1983; Hoppe and Reichert 1987; Fromont 1994; Mercurio et al. 2007). From an ecological point of view, sponge sexual reproduction is widely identified with timing of larval release, because the idea of “effective reproduction” is often associated with the production of dispersing embryos or larvae. However, that ecological perspective disregards the intricacies of some underlying processes, such as gametogenesis and fertilization, which may play a relevant role in determining the timing of larval production. In externally-developing demosponges, the timing of effective reproduction can be assimilated to that of gametogenesis and embryogenesis, because these 2 processes occur very fast (days to weeks). As a consequence most externally-developing demosponges can be said to release gametes and produce

embryos during a short period once a year, with relative high synchrony at the population level (reviews: Fell 1974, 1983; Reiswig 1983; Boury-Esnault and Jamieson 1999; Usher et al. 2004). Brooding demosponges show a more complicated pattern. In temperate latitudes, populations of most brooding demosponges concentrate larval release in one annual period, which extends for several weeks, usually during the warm season (e.g., Lévi 1956; Wapstra and van Soest 1987; Maldonado and Young 1996; Corriero et al. 1998; Maldonado and Uriz 1998; Ereskovsky 2000; Mariani et al. 2000, Maldonado 2006). Alternatively, some sublittoral and intertidal brooding demosponges release small quantities of larvae through the year, though a peak of massive release occurs only once or twice a year, usually during the warm season (e.g., Bergquist and Sinclair 1968; van Koolwijk 1982; Zea 1993). The maximum asynchrony at larval release is found in some tropical and subtropical sponges, which may incubate variable amounts of embryos at any time over the year (e.g., Storr 1964; Bergquist 1978; Kaye and Reiswig 1991; Ilan and Loya 1990). On the basis of the available studies, it is usually assumed that reproductive activity is maintained over the year in the tropics because of the relatively high and unchanging seawater temperatures, while drastic seasonal changes in temperature are thought to be responsible for the discontinuous reproductive patterns reported in temperate latitudes (e.g., Storr 1964; Sarà and Vacelet 1973; Elvin 1976; Fell 1983; Simpson 1984; Wapstra and van Soest 1987; Kaye and Reiswig 1991; Fromont 1994).

By investigating the life cycle of a temperate homosclerophorid demosponge, *Corticium candelabrum* Schmidt 1862, we describe the dynamics and ultrastructure of gametogenesis and embryogenesis, as well as their relationship with seawater temperature. We show that the sponges remain gametogenetically active the entire year, irrespective of seawater temperature and despite the fact that their cinctogastrula larvae are exclusively produced during a narrow time window in the Mediterranean summer.

Material and Methods

Study species

Whether *Corticium candelabrum* is a cosmopolitan species or a Mediterranean endemism is unresolved, although the latter option is postulated as more likely (Muricy and Díaz 2002). Five other species occur in the genus, known from the Eastern Atlantic,

the Caribbean, the Indian Ocean, the Australian Pacific, and New Caledonia (Muricy and Díaz 2002). The Mediterranean *C. candelabrum* individuals are small, orangish-brown, cushion-shaped to lobate sponges, measuring up to 1.5 cm in thickness and up to 10 cm in their largest diameter. The studied population of *C. candelabrum* occupies the 8-20m depth range along the sublittoral rocky cliff of the Catalan Coast (Spain, northwestern Mediterranean).

Dynamics of abundance and size of reproductive elements

For a long-term monitoring of reproductive activity in the population, we tagged five large and presumably mature individuals at random, which were sampled monthly, from October 2003 to December 2004. Diving with scuba and using surgical scissors, we collected a small tissue piece (approx. 1 x 0.5 x 0.5 cm) from each sponge at each sampling time. In no case tissue collection caused death of the sampled sponges or perceivable functional damage. When samples from the tagged individuals revealed that gametogenesis activity was about to peak in the population, which happened in summer, we increased both sampling frequency (10-day intervals) and number of sampled individuals (N = 30). At each time of "summer sampling", we collected tissue pieces from the 5 tagged individuals, as well as from 25 non-tagged sponges at random, irrespective of whether they were sampled in a previous dive.

Tissue samples for optical microscopy were maintained in ambient seawater for transportation to the laboratory (1 to 2 h) and fixed in 4% formaldehyde in seawater for 24 h. Then, samples were desilicified with 5% hydrofluoric acid for 1.5 h, rinsed in distilled water, dehydrated through a graded ethanol series (70%, 96%, 100%), cleared in toluene, and embedded in paraffin to cut them into 5 μm-thick sections using an Autocut Reichert-Jung microtome 2040. After deparaffining with xylene, sections were stained with Hematoxylin-PAS and observed through a Zeis Axioplan II compound microscopy connected to a Spot Cooled Color digital camera. To count and measure the various reproductive elements (i.e., spermatic cysts, oocytes, pre-gastrular solid embryos, and post-gastrular hollow embryos) per tissue area unit, we took 2 pictures (x100) of each of 2 non-serial sections per individual. Likewise, pictures of tissue were taken at least 240 μm from each other to avoid overlapping of reproductive products leading to overestimation. The 4 pictures provided a total surveyed area of 7 mm^2 per individual. We determined number of reproductively active sponges overtime and

estimated number, area, and largest diameter of each reproductive element, using the public domain ImageJ Software (http://rsb.info.nih.gov/ij/index.html) on the digital histological images. Then, we estimated average density (mean number per unit area ± SD; for tagged individuals only), size, and mesohyl occupancy (percentage area) for each type of reproductive product in the reproductive individuals.

Given that oocyte development was found to be an unexpectedly long process, we approached the study of oocyte size distribution (in 25 μm size classes) and oocyte abundance over a year cycle by repetitive sampling of the tagged individuals only. This method was expected to provide a more accurate description of the dynamics of oocyte cohorts than non-repetitive, random sampling. We also investigated the relationship between cell and nucleus size during oocyte growth by measuring these parameters in a total of 129 oocytes selected at random from the annual pool of samples provided by the 5 tagged individuals. We used Pearson correlation (r^2) to examine the relationship between oocyte and nucleus size, which were normally-distributed variables.

Reproductive activity vs. seawater temperature

We measured seawater temperature (± 0.5 ºC) at the sampling sites monthly, placing the underwater thermometer (Suunto) close to the rocky walls where the sponges grow. The potential relationship between temperature and reproductive activity was examined by plotting monthly temperature values versus estimated density (abundance per mm^2) of reproductive products.

Ultrastructural study

Transmission electron microscopy (TEM) was used when needed to describe the ultrastructure of gamete production. Tissue samples for TEM observation were fixed within 1 hour after collection, according to the protocol detailed elsewhere (Maldonado et al. 2003, 2005). Primary fixation was in 2.5% glutaraldehyde in 0.2M Milloning's phosphate buffer (MPB) and 1.4M sodium chloride for 1 h. Samples were then rinsed with MPB for 40 min, post-fixed in 2% osmium tetroxide in MPB, dehydrated in a graded acetone series, and embedded in Spurr's resin. Ultrathin sections obtained with an Ultracut Reichert-Jung ultramicrotome were mounted on gold grids and stained with 2% uranyl acetate for 30 min, then with lead citrate for 10 min (Reynolds 1963). Observations were conducted with a JEOL 1010 transmission electron microscope

(TEM) operating at 80 kV and provided with a Gatan module for acquisition of digital images.

Results

Dynamics of abundance and size of reproductive elements

Examination of histological sections from 149 individuals of *C. candelabrum* confirmed that this sponge is simultaneously hermaphroditic.

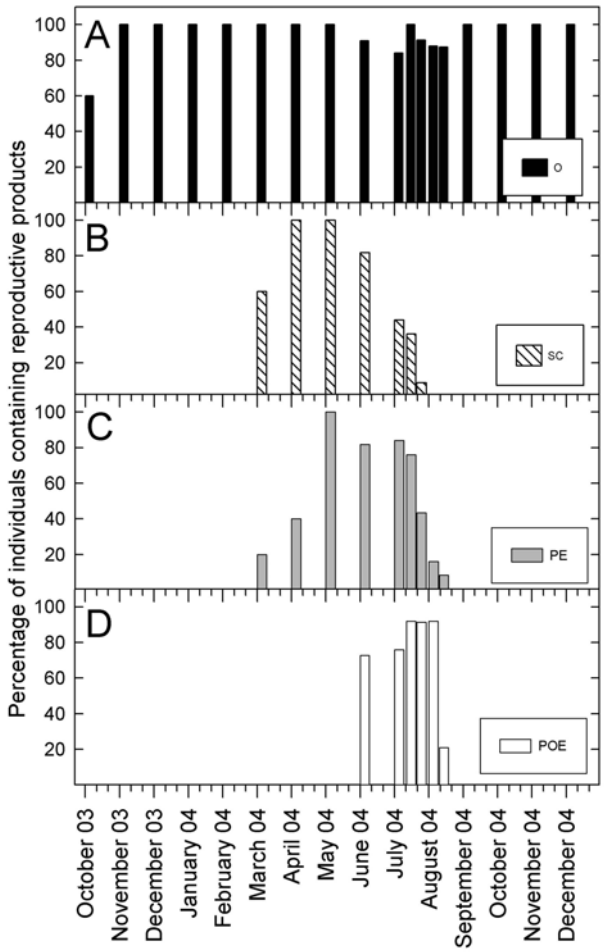

Figure 1. Abundance (percentage) of individuals containing reproductive products over a year cycle (October 2003 to December 2004). **(A)** oocytes (O), **(B)** spermatic cysts (SC), **(C)** pregastrular embryos (PE), and **(D)** postgastrular embryos (POE). Note that during summer months, sampling frequency increased from 1-month to 10-day intervals and number of sampled individuals from 5 to 30.

Developing oocytes occurred at all sampling times over the year, while sperm production was restricted to late spring and early summer (Fig. 1A).

Over a year cycle, all 5 tagged individuals engaged in gamete production (Fig. 1A, B). Nevertheless, several samplings during the peak of reproductive activity in summer revealed that about 10% of additional 25 individuals taken at random contained no gamete.

These individuals were usually quite small (< 3 cm^2 approx.) and could be sexually immature. Spermatic cysts located underneath the pinacoderm of the canals, usually around growing oocytes and embryos (Fig. 2). Likewise, oocytes consistently located in the mesohyl immediately below the endopinacoderm of the exhalant canals (Fig. 2). Choanocyte chambers were scarce in the mesohyl areas where oocytes abounded, in contrast to which is known for other homosclerophorids (Gaino et al. 1986a). Interestingly, production of oocytes in *C. candelabrum* was a continuous process with increased production rates from October to January, coincidental with a decline in temperature (Fig. 3).

The highest average density of oocytes (7.1 ± 2.9 oocytes per mm^2) in the tissue occurred in February, prior to the onset of spermatogenesis (Fig. 3). At this time, we estimated that about 58.6% of oocytes were mature or nearly mature. It is noteworthy that we detected a decrease in oocyte density in March, disrupting the expected dynamics over time (Fig. 3). We suspect that such a decrease is an artefact caused by deficient fixation of March samples, which hindered identification of the smallest oocytes under the compound microscope and favoured a possible underestimation of average oocyte density. The lowest average density of oocytes (0.5 ± 0.5 oocytes per mm^2) occurred in late June (Fig. 3), immediately after a peak in production of small new embryos, which we interpret as resulting from a fertilization peak in mid June. Therefore, it appears that nearly all large oocytes were fertilized in June, being left in the tissue only newly produced (< 90 μm) oocytes (Fig. 4).

The study of size dynamics corroborated that oocytes as small as 15 μm in diameter (i.e., the minimum size for reliable identification by light microscopy) occurred at any month over the year, but more abundantly from October 2003 to April 2004 (Fig. 4). Likewise, average diameter increased progressively from August of one year to May of the next one, when oocytes reached 125 to 175 μm in diameter (Fig. 5).

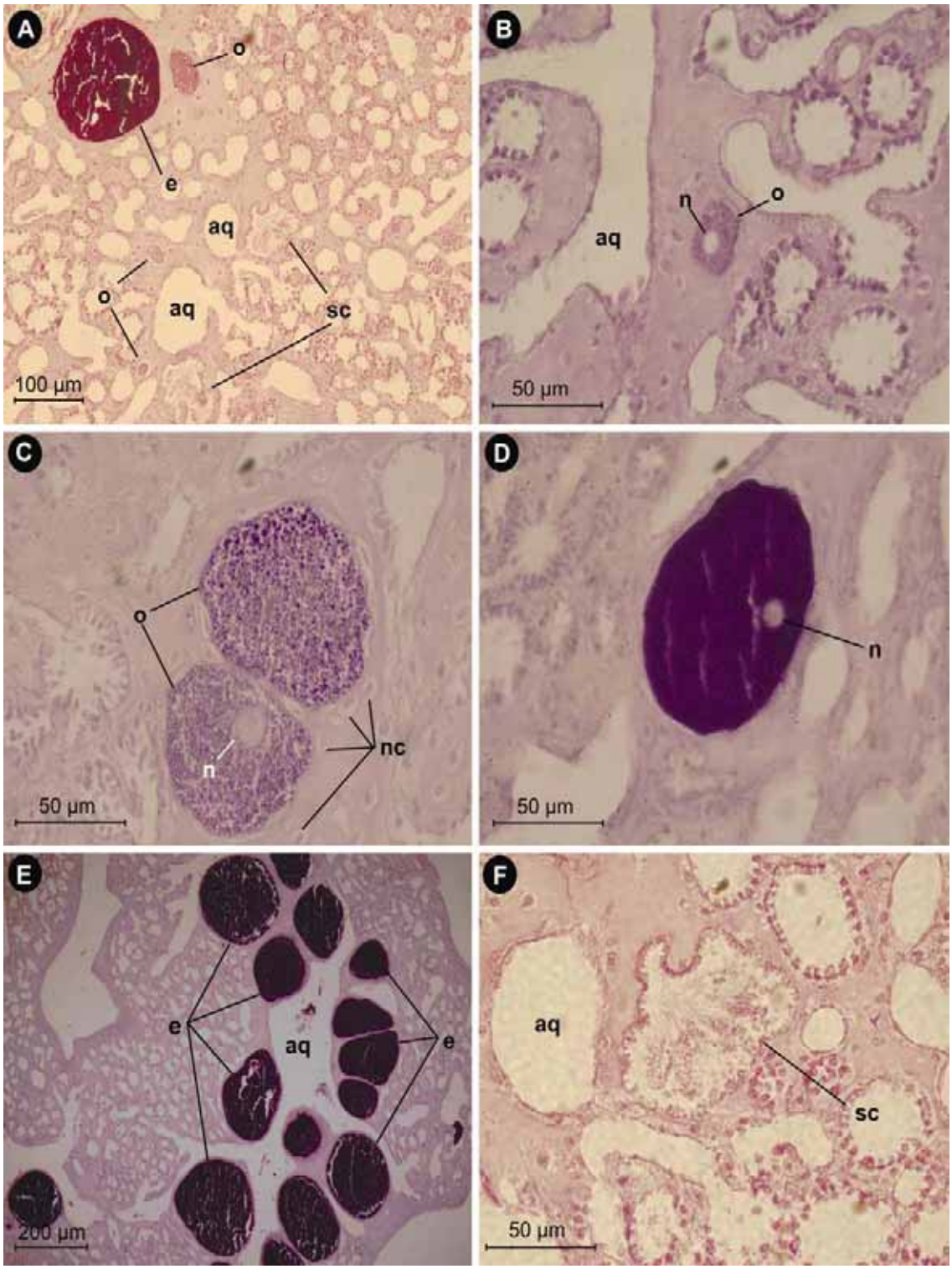
A
o
e
aq
o
aq
sc
100 µm
B
aq
n
o
50 µm
C
o
n
nc
50 µm
D
n
50 µm
E
e
aq
e
200 µm
F
aq
sc
50 µm

Figure 2. Light microscopy observations of gametogenesis and embryogenesis. **(A)** Co-occurrence of early-stage oocytes (o), embryos (e), and spermatic cysts (sc) in the mesohyl of the sponge, close to the aquiferous canals (aq). **(B)** Early-stage oocyte (o) with an eccentric nucleolate nucleus (n), located between 2 aquiferous canals (aq). **(C)** Several nurse cells (nc) around mid-stage oocytes (o). Note the eccentric situation of the nucleolate nucleus (n). **(D)** Late-stage oocyte with a deeply-stained cytoplasm indicating on-going vitellogenesis and an eccentric nucleus (n). **(E)** High abundance of embryos (e) around an exhalant canal (aq). **(F)** Spermatic cyst (sc) close to an aquiferous canal (aq), showing spermatozoa with the tail directed towards the lumen.

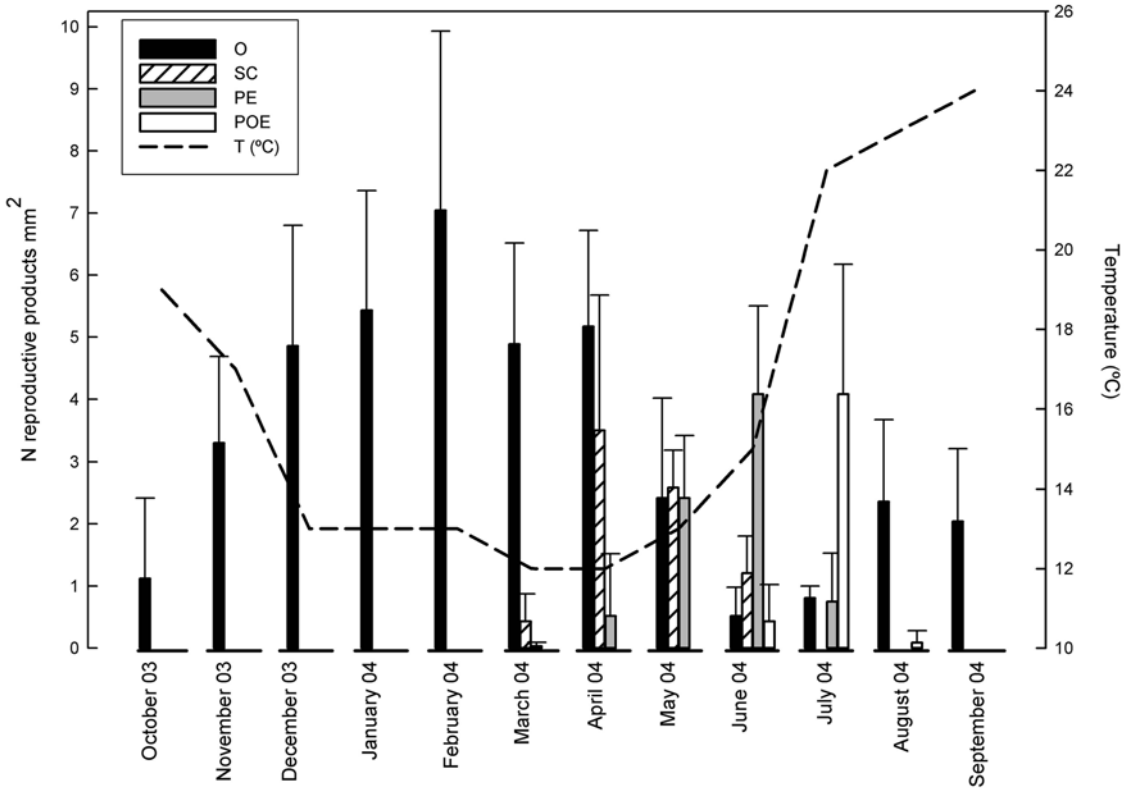

Figure 3. Density (± standard deviation) of reproductive products (O = oocytes, SC = spermatic cysts, PE = pregastrular embryos, and POE = postgastrular embryos) in the sponge tissue of 5 tagged individuals over a year cycle (October 2003 to September 2004) versus seawater temperature.

These patterns of abundance and size suggest that, despite moderate production of new oocytes at any time over the year, a general cycle of oogenesis occurred, starting in August and ending with fertilization in July of the following year. In May, we also noticed few, extremely large (200-250 μm) oocyte-like bodies (Fig. 4), which could be either "true" oocytes or 2-cell blastula stages with a cleavage furrow that was not evident under optical microscopy. At all growth stages, oocytes showed a relatively large nucleolate nucleus, ranging from 7 μm in diameter in the smallest oocytes to 25 μm in largest ones. We detected a positive correlation ($N = 129$; $r^2 = 0.7$; $P < 0.05$) between nucleus and oocyte diameters, indicating that nuclear enlargement is directly proportional to cell growth (Fig. 6).

Spermatic cysts were first detected in March, upon density of oocytes reached its maximum (Fig. 3). Average density of cysts (cysts per mm^2) increased from 0.4 ± 0.4 on its first detection to the maximum value (3.5 ± 2.2) in just 1 month. Then, density values gradually decreased until complete disappearance in early August (Fig. 3). Average size (largest diameter) of cysts raised from 40.8 ± 7.8 μm in March to 60.4 ± 10.8 μm in May (Fig. 5).

Early pre-gastrular embryos (solid blastula stages) were first detected in March and seen in mid-August for the last time (Figs 1C, 2). Average density of pre-gastrular embryos, which was 0.03 embryos mm^{-2} at their appearance (in 1 individual only) in March, increased to the maximum value of 4.1 ± 1.4 embryos mm^{-2} in late June (Fig. 3). Because there was virtually no difference in maximum average density between mature oocytes (4.1 oocytes mm^{-2}) recorded in February and pre-gastrular embryos (4.1 embryos mm^{-2}) recorded in June, we estimated the success of internal fertilization as 99.3% at the population level.

Formation of new embryos suggested that fertilization extended from March to July, peaking from late May to mid June and decreasing dramatically along June, as indicated by low embryo production (0.7 ± 0.8 embryos mm^{-2}) in July. During the pre-gastrular phase, embryos experienced just histological transformations, attaining virtually no significant increase in size (Fig. 5). Post-gastrular (hollow) embryos first appeared in late June (Figs 1D, 2), showing maximum density (4.1 ± 2.1 embryos mm^{-2}) during the second week of July (Fig. 3).

They were finally released as free-swimming cinctogastrula larvae during early August. The post-gastrular phase was characterized by a progressive decrease in

average embryo size (Fig. 5). Average density of pre-gastrular and post-gastrular were nearly identical values (Fig. 3), revealing that there was no substantial embryo mortality during the brooding process. Reproductive products occupied a relatively modest percentage (< 12%) of the mesohyl and never disrupted the histological organization of the sponges, not even during the peak of reproduction (Fig. 7).

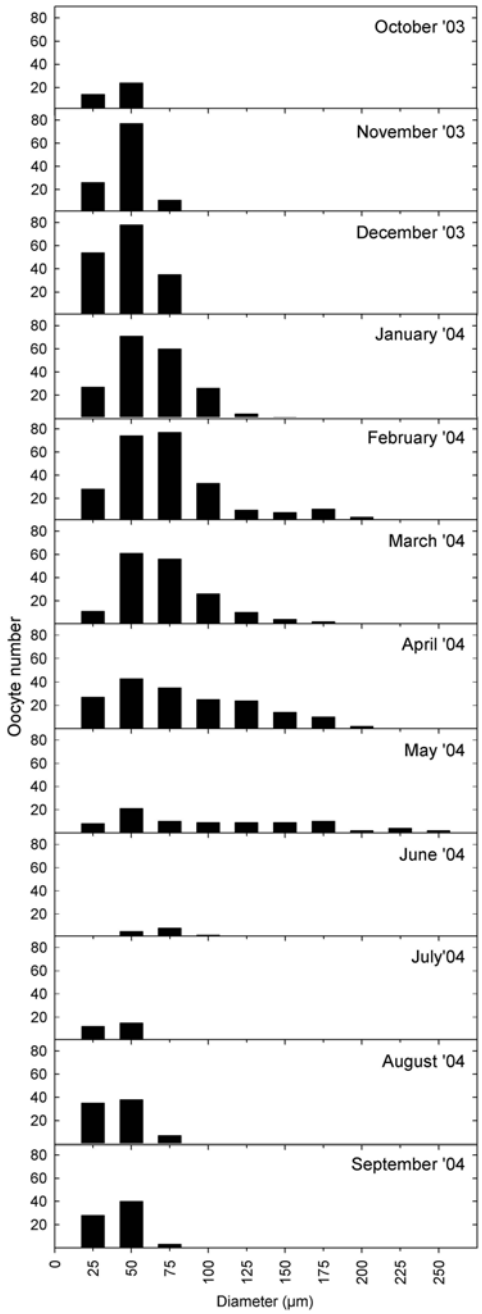

Figure 4. Size distribution of oocytes found in the sponge tissue of 5 tagged individuals over a year cycle (October 2003 to September 2004).

Spermatic cysts took minimum mesohyl space, reaching the maximum occupancy (0.9%) in May. At no time mesohyl occupancy by oocytes was nil (Fig. 7), ranging from 0.1% in mid July to 2.9% in February. Both pre-gastrular and post-gastrular embryos, when present, occupied up to 7.7% (Fig. 7). Though post-gastrular embryos were somewhat larger than pre-gastrular ones (Fig. 5), the first ones did not reach a substantially higher occupancy than the latest ones because they started soon being released gradually as larvae.

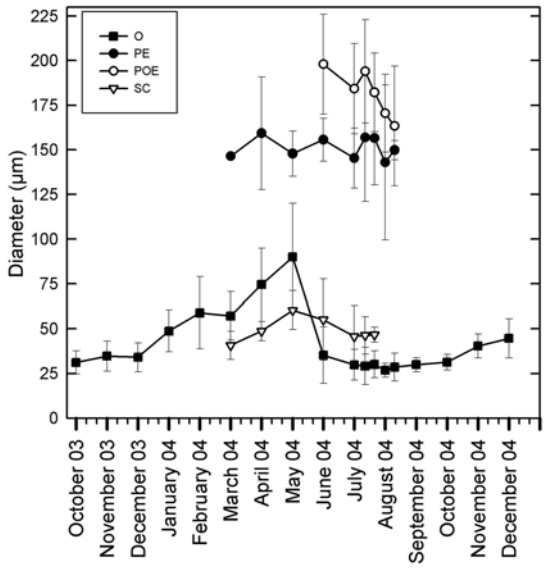

Figure 5. Size (mean ± SD) dynamics of reproductive products (O = oocytes, SC = spermatic cysts, PE = pregastrular embryos, and POE = postgastrular embryos) over a year cycle (October 2003 to December 2004). Note that during summer months, sampling frequency increased from 1-month to 10-day intervals and number of sampled individuals from 5 to 30.

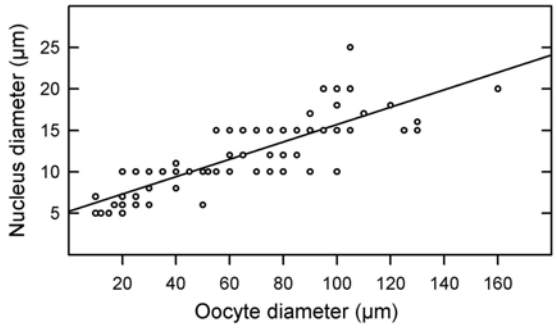

Figure 6. Relationship between oocyte diameter (µm) and nucleus diameter (µm). A significant Pearson correlation coefficient (r^2 = 0.668; P < 0.05; N = 129) indicates that oocyte growth involves a parallel increase in nuclear size.

Reproductive activity vs. seawater temperature

The relationship between seawater temperature and gametogenic/embryogenic processes was complex. Temperature did not appear to be the main cue triggering oogenesis, since new oocytes were produced every month, under conditions that spanned a wide range of temperature values (12 to 24 ºC). Nevertheless, production rate of oocytes increased markedly from October to December, coincidentally with decreasing temperature (Fig. 3). Surprisingly, unlike in most known demosponges, most oocytes grew during the coldest period of the year (January to April). Likewise, spermatogenesis started in the coldest month, just before the spring rising of temperature (Fig. 3), and extended over a time period that involved both cold and warm seawater. On the other hand, the onset of embryogenesis coincided with the rise of temperature. Larval release occurred under conditions of maximum seawater temperature (Fig. 3).

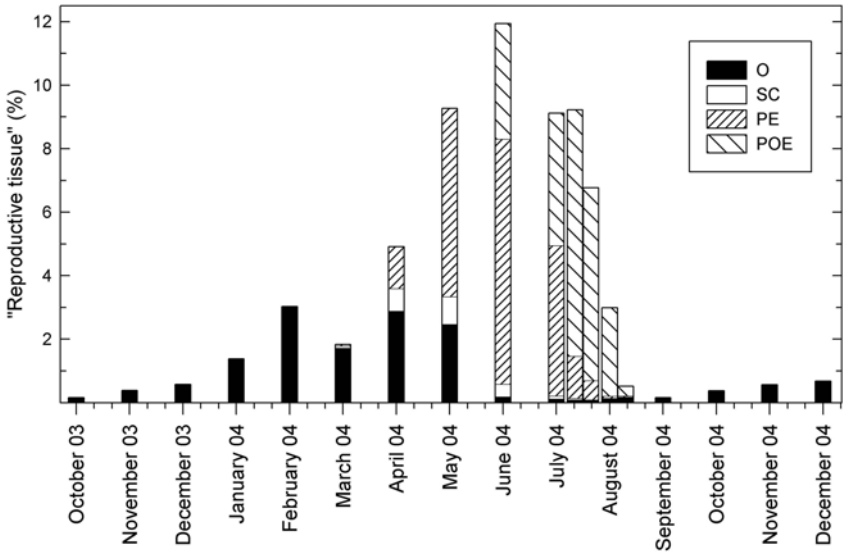

Figure 7. Occupancy (%) of sponge tissue by reproductive elements (O = oocytes, SC = spermatic cysts, PE = pregastrular embryos, and POE = postgastrular embryos) over a year cycle (October 2003 to December 2004). Note that during summer months, sampling frequency increased from 1-month to 10-day intervals and number of sampled individuals from 5 to 30.

Ultrastructure of oogenesis

The smallest identifiable oocytes consistently located in the mesohyl immediately beneath the endopinacoderms (Fig. 2A), probably as the result of transdifferentiation of migrating archaeocytes. During oogenesis, abundant amoeboid nourishing cells (nurse cells) migrated towards the surrounds of growing oocytes (Fig. 8A). We have identified 2 types of nurse cells, one containing great abundance of bacteria in cytoplasmic vacuoles (Fig. 8B), and the other mostly carrying incipient yolk granules, as well as putative proteinaceous and lipid precursors of yolk (Figs 8C-D). Both cell types, which ranged in size from 11 to 15 μm, had a nucleolate nucleus of about 3 to 3.5 μm in diameter.

Figure 8. Nurse cells and early-stage oocytes. **(A)** Nurse cells (nc) surrounding a mid-stage oocyte (o). **(B)** Enlarged area of Fig. 8A showing a nurse cell charged with bacteria (b), close to an oocyte charged with a mix of incipient (proteinaceous) yolk granules (py) and complex yolk granules (cy). **(C)** Nurse cell charged with incipient (proteinaceous) yolk granules (py) and putative yolk precursors (yp) contacting the membrane of an early-stage oocyte. Note incipient yolk granules (py) along with lipid droplets (l) scattered through the oocyte cytoplasm. **(D)** Nurse cell containing a mix of proteinaceous yolk granules (py) and bacteria (b). **(E)** Detail of the eccentric nucleus (n) of an early-stage oocyte. The cytoplasm contains sparse lipid droplets (l), small proteinaceous yolk granules (py), and smaller particulate inclusions that are regarded as yolk precursors (yp). Note incipient accumulation of intercellular bacteria (ib) around the oocyte membrane. **(F)** Detail of a proteinaceous yolk granule that has not incorporated lipid compounds yet. It is surrounded by incipient yolk granules (py), diverse particulate yolk precursors (yp), and electron-clear vacuoles (v).

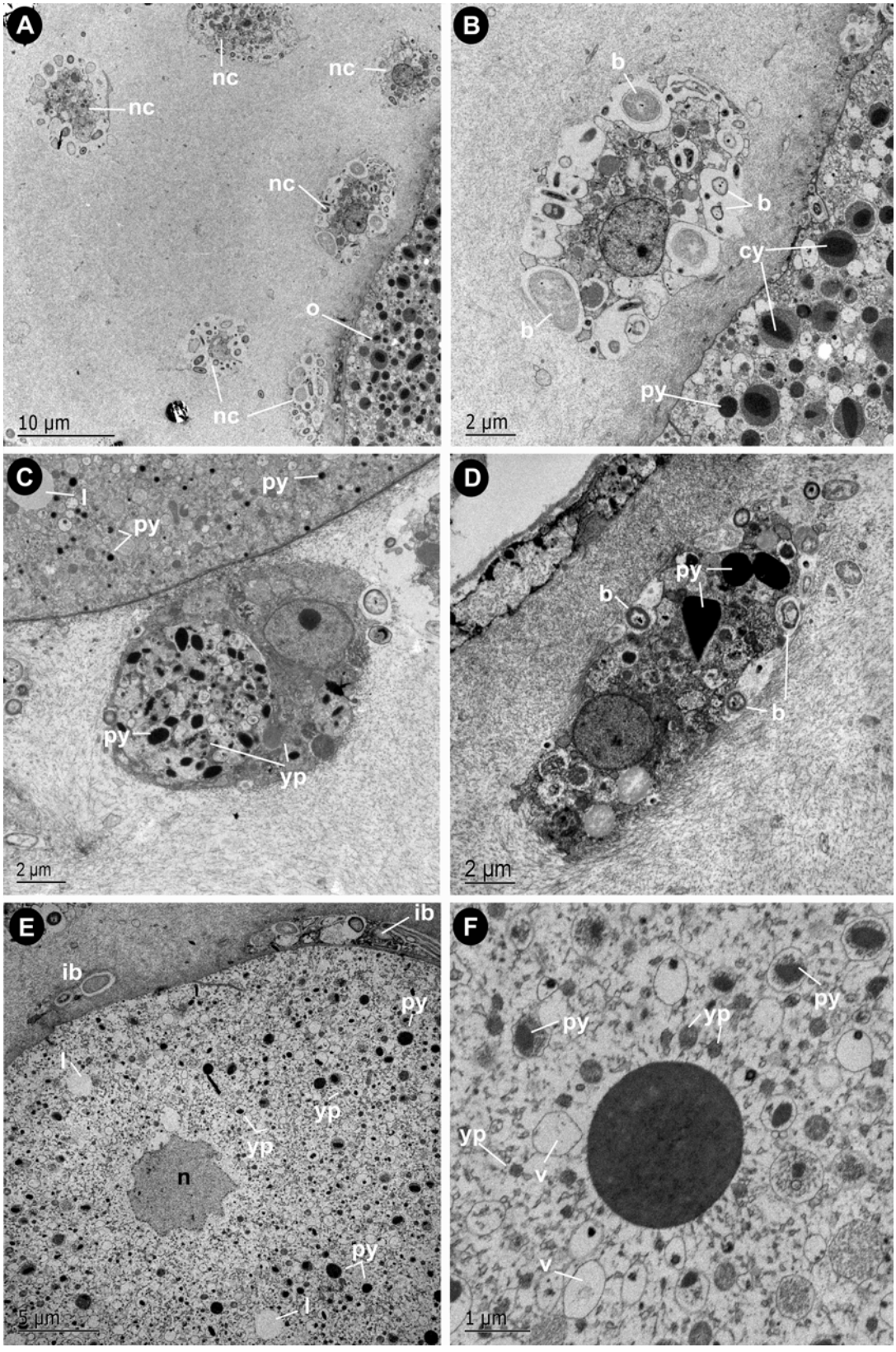
A
nc
nc
nc
nc
o
nc
10 µm
B
b
b
cy
b
py
2 µm
C
l
py
py
py
yp
2 µm
D
py
b
b
2 µm
E
ib
ib
py
l
yp
yp
n
py
l
5 µm
F
py
py
yp
yp
v
v
1 µm

Early-stage oocytes showed a cytoplasm charged with electron-clear vesicles, digestive vacuoles, and small round yolk granules (Figs 8C, E-F). At this stage, yolk granules, which were sparse, consisted mostly of proteinaceous material, with no lipids (Fig. 8F). Initially the oocyte nucleus was central (Fig. 2A), but once oocytes grew larger than approximately 20 μm, it became eccentric, with a very homogeneous arrangement of chromatin (Figs 2B-C, 8E). In mid stage-oocytes (Fig. 9A), the number of cytoplasmic inclusions increased and the proteinaceous yolk granules became ellipsoidal (Fig. 9B), though they still did not incorporate lipidic compounds.

When oocytes grew larger than 50 μm, they contained mostly "mixed" yolk granules that combined electron-clear lipidic compounds and electron-dense, paracrystalline proteinaceous components (Figs 8B, 9C). Their cytoplasm also harboured scattered lipid droplets (Fig. 9C), glycogen granules (Fig. 9D), and heterogeneous inclusions of either pseudo-digested materials or yolk precursors (Fig. 9E). Intercellular bacteria accumulated progressively around the growing oocytes (Figs 8E, 9A), forming a relatively thick layer that surrounded late-stage oocytes (Figs 9C, F). The bacterial layer became externally limited by a thin basement-membrane-like condensation of collagen microfibrils (Figs 9C, F). It is worth noting that while early-stage oocytes engulfed isolated bacteria and cyanobacteria only occasionally (Figs 10A-B), late-stage oocytes phagocytosed large amounts of bacteria that were digested within large (5-7 μm) vacuoles in the peripheral cytoplasm (Figs 10C-D). Though some nurse cells contained yolk granules, most yolk appeared to be synthesized "de novo" by the oocytes themselves, using both phagocytosed bacteria and precursors provided by the nurse cells. Interestingly, unlike in other homosclerophorids, oocytes of *C. candelabrum* lacked both interdigitations and microvilli at any stage.

In oocytes of 2 different individuals, we documented the emission of a putative polar body. We assume that it was the second polar body of their meiotic division, since oocytes were very large and about to complete their vitellogenesis (Fig. 10E). In these bodies, we confirmed occurrence of small yolk granules (1-2 μm) nearly identical to those in the late oocytes. Nevertheless, we never found the typical nuclear material characterizing polar bodies (perhaps because very few sections of bodies were available). Both bodies were oval. One, measuring 4 μm in largest diameter, laid within

the bacterial layer that surrounds the oocyte (Fig. 10E); the other, measuring 14 μm, located in the mesohyl immediately external to the bacterial layer (Fig. 10F).

Ultrastructure of spermatogenesis

Spermatic cysts appeared in those mesohyl areas where oocytes were already developing (Figs 2A, F). They were irregular in shape (Fig. 2E) and externally limited by a basement membrane (Fig. 11A), lacking cellular follicle. They showed a stratified organization from the basement membrane to the lumen (Fig. 11A), with concentric, multilayered cell strata comprised of spermatogonia (Fig. 11B), primary spermatocytes (Figs 11B-C), secondary spermatocytes (Fig. 11D), and spermatids (Figs 11E-F), respectively. Cells in the cyst were flagellated at all stages of spermatogenesis, with the tail oriented towards the lumen (Figs 11A-F). All cells were also interconnected by cytoplasmic bridges (Figs 12A-D) resulting from incomplete cytoplasm divisions during spermatogenesis, as typically described for other metazoans.

The outer stratum of cysts, made of pseudo-cubic to round cells (3-4.5 μm) of 2 types, was usually bi-layered (Figs 11A, 12A, B). There were cells with a large nucleolate nucleus (2-2.5 μm), which corresponded to spermatogonia (Figs 11B, 12A, 13A). There were also cells with a similar nucleus but showing the synaptonemal complexes (chromosomal synapses) typical of Prophase I (Figs 11B, 12B, 13A-B), which corresponded to primary spermatocytes. Spermatogonia were suspected to derive from choanocytes for several reasons. They both had a similar cell size. Like choanocytes (Fig. 13D), spermatogonia showed a prominent nucleolus in the nucleus (Fig. 11B), which disassembled at the onset of meiosis when they became primary spermatocytes (Figs 11B-C, 12B). The flagellum, which lacked rootlet through the whole spermatogenesis, had a basal body provided with a simple basal foot and an accessory centriole laying perpendicular to that of the basal body (Figs 13C), as typically occurring in choanocytes (Figs 13D). Likewise, spermatogonia and choanocytes had a well developed Golgi apparatus located at the distal side of the nucleus, adjacent to the ciliary basal body (Fig. 13C). Because the basal stratum of the cysts was formed mostly by primary spermatocytes, we assumed that the spermatogonia layer was ephemeral, rapidly transforming into primary spermatocytes. Both spermatogonia and primary spermatocytes contained several mitochondria, which

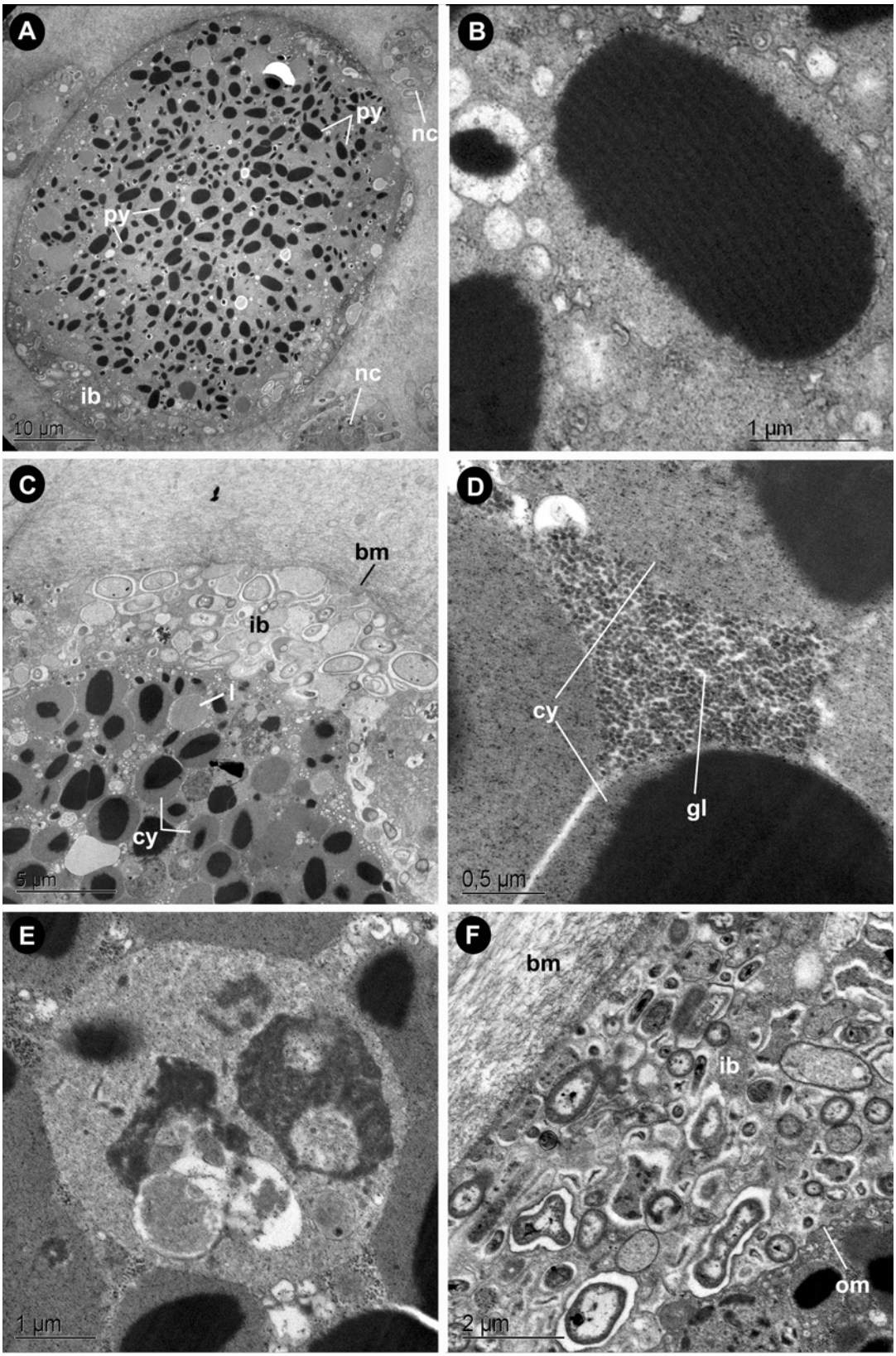
A
py
nc
py
nc
ib
10 µm
B
1 µm
C
bm
ib
l
cy
5 µm
D
cy
gl
0,5 µm
E
1 µm
F
bm
ib
om
2 µm

Figure 9. Mid- and late-stage oocytes. **(A)** General view of a mid-stage oocyte charged with abundant ellipsoidal proteinaceous yolk granules (py), and surrounded by mesohyl bacteria (ib) and several nurse cells (nc). **(B)** Detail of an ellipsoidal, proteinaceous yolk granule in a mid-stage oocyte, showing its paracrystalline structure. **(C)** Detail of a late-stage oocyte showing complex yolk granules (cy) and lipid droplets (l). A relatively thick bacterial accumulation develops around the oocytes (ib), being externally limited by a basement-membrane-like condensation (bm) of collagen microfibrils. **(D)** Abundant glycogen (gl) granules between complex yolk granules (cy) in the oocyte cytoplasm. **(E)** Heterogeneous inclusions of either pseudo-digested materials or yolk precursors in a late-stage oocyte. **(F)** Detail of the thick bacterial accumulation (ib) formed between the membrane (om) of a late-stage oocyte and the basement-membrane-like (bm) condensation of collagen microfibrils.

engaged in fusion (Fig. 13B, C). Such a mitochondrial fusion process extended through the whole spermatogenesis, so that mitochondria progressively decreased in number and increased in size, leading to a single, large mitochondrion in the mature spermatozoon.

Secondary spermatocytes, which result from completion of the first meiotic division, occurred in the cyst internally to primary spermatocytes (Fig. 11A). They were round cells, slightly smaller (about 2.5-3 μm in diameter) than spermatocytes I, because part of their cytoplasm was exocytosed during the cytokinesis (Figs 11D, 12C). Their nucleus became slightly oval, showing an incipient condensation of chromatin (Fig. 11D). Their fusing mitochondria became scarcer and larger (Fig. 14A) than in spermatocytes I. The Golgi apparatus, still clearly visible, started forming the acrosomal vesicle (Fig. 14C). A large electron-clear vacuole of unknown function also appeared in their cytoplasm (Figs 11D, 14C). Spermatids, which are already haploid cells resulting from completion of the second meiotic division, made a multilayered stratum internal to that of secondary spermatocytes (Fig. 11A).

Spermatids were about the same size than secondary spermatocytes, but showed an oval nucleus with highly condensed chromatin, except for a small, electron-clear central area (Figs 11E-F, 14A). The nucleus had a small indentation in the region adjacent to the flagellum insertion (Figs 11E-F). Alar sheets and anchoring points linked the typical 9 + 2 basal body of the flagellum to the surrounding cell membrane (Figs 14A-B). The cytoplasm usually contained a single, large mitochondrion and showed the

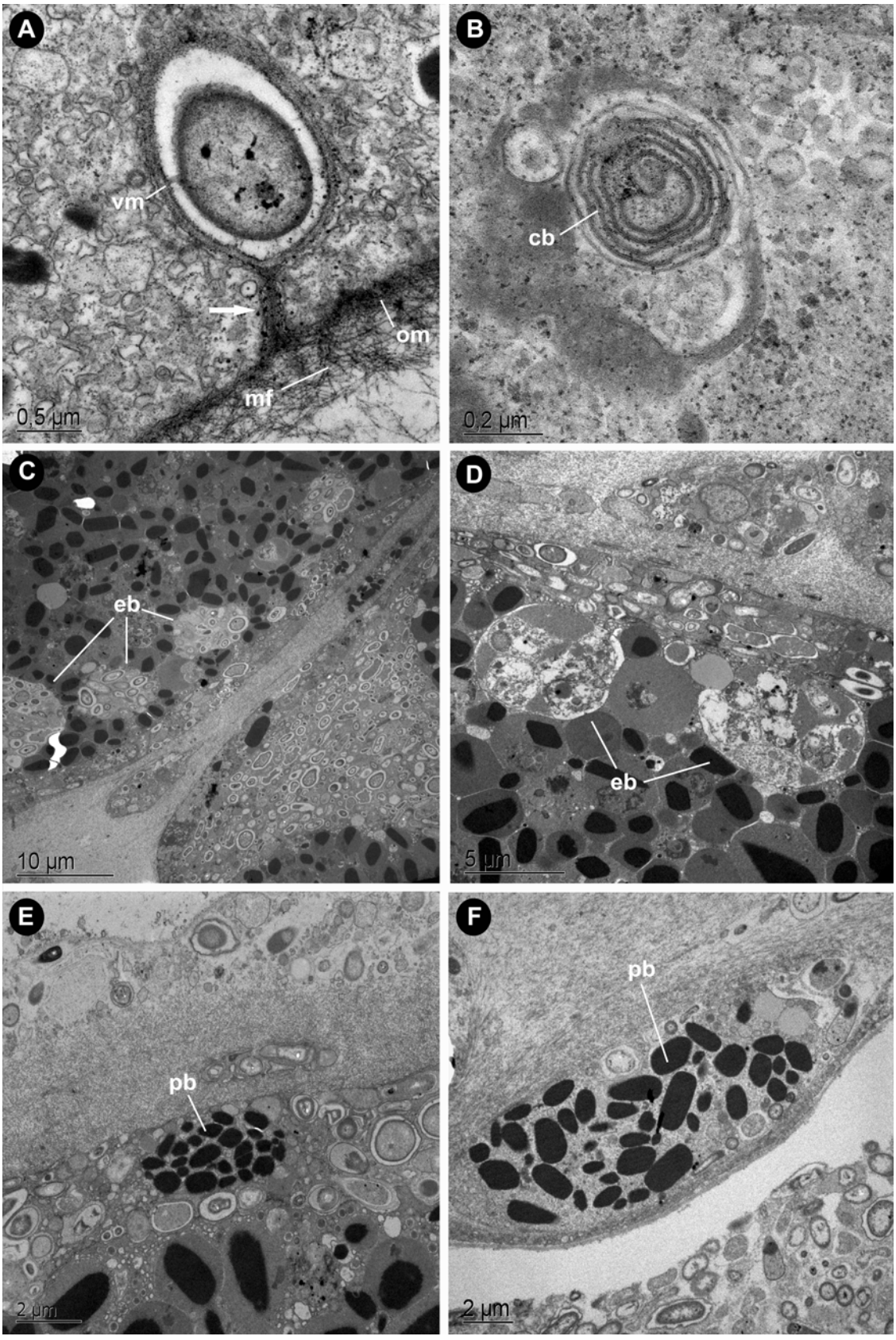
A
vm
om
mf
0,5 µm
B
cb
0,2 µm
C
eb
10 µm
D
eb
5 µm
E
pb
2 µm
F
pb
2 µm

Figure 10. Bacterial engulfement and polar bodies. **(A)** Early-stage oocyte showing a bacterium recently phagocytosed, as indicated by the connection (arrow) between the membrane of the vacuole (vm) and the oocyte oolemma (om). Note the condensation of collagen microfibrils (mf) around the oocyte. **(B)** Early-stage oocyte showing a vacuole with diverse material, including a pseudo-digested cyanobacterium (cb). **(C)** Engulfment of groups of bacteria (eb) by a late-stage oocyte. **(D)** Digestion of groups of bacteria (eb) engulfed by a late-stage oocyte. **(E-F)** Putative polar bodies (pb) jettisoned by late-stage oocytes as the result of their second meiotic division.

electron-clear vacuole that appeared at the spermatocyte-II stage (Figs 11E-F, 14C). The Golgi apparatus disassembled after giving rise to the acrosome (Fig. 14D-E). In transversal sections of spermatids, the acrosome often appeared as two acrosomal vesicles, one at each side of the cell (Figs 12D, 14F). Indeed, the vesicles corresponded to each end of a single C-shaped acrosomal body (Figs 11E, 14A, D-F). It was a long (2 μm) and narrow (200-300 nm), tubular structure that extended along the anterior (opposite the flagellum insertion) cell pole.

Spermatids, like spermatocytes, were connected by cytoplasmic bridges (Figs 12D, 14A). Cell connections were likely closed at the very moment in which spermatids became functional spermatozoa. However, we could not corroborate this issue, since no studied cysts contained free-swimming spermatozoa. We found that some spermatids had the accessory centriole migrated to the cell side opposite the flagellum insertion (Fig. 11F), a feature suggesting an imminent cell division (e.g. Buss 1987). Therefore, spermatids may be able to further divide themselves to produce mature spermatozoa.

Post-gametogenic observations

Although release of free-swimming spermatozoa was never observed, we documented a spermatozoon swimming within a choanocyte chamber in June samples (Fig. 15A-B), as well as a putative spermiocyst inside a presumptive carrier cell located immediately adjacent to a choanocyte chamber (Fig. 15C). Size and general organization of the carrier cell were similar to those of choanocytes, including the large digestive vacuole typically found in choanocytes (Figs 15C-D). Therefore, we suspect that the carrier cell

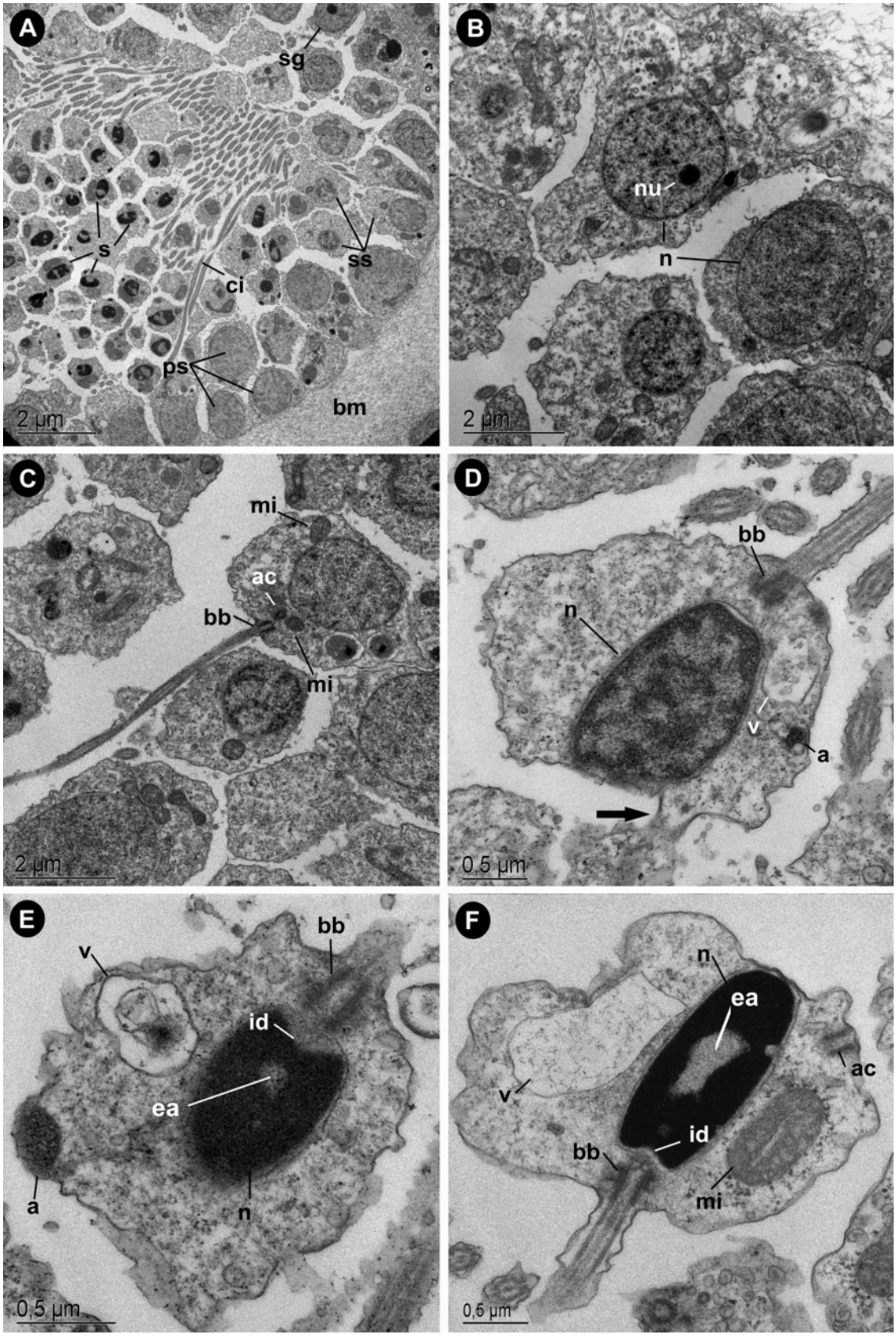
A
sg
s
ss
ci
ps
bm
2 µm
B
nu
n
2 µm
C
mi
ac
bb
mi
2 µm
D
bb
n
v
a
0,5 µm
E
bb
v
id
ea
a
n
0,5 µm
F
n
ea
ac
v
id
bb
mi
0,6 µm

Figure 11. Overview of spermatogenesis stages. **(A)** General view of a spermatic cyst enveloped by a basement-membrane-like structure (bm) and containing spermatogonia (sg), primary spermatocytes (ps), secondary spermatocytes (ss), and spermatids (s) with the flagellum (ci) oriented towards the cyst lumen. **(B)** Detail of a peripheral, nucleolate (nu) spermatogonium and a primary spermatocyte with a large nucleus (n). **(C)** Stratum of primary spermatocytes with a spermatocyte showing several small mitochondria (mi), the basal body (bb) of the flagellum, and the accessory centriole (ac). **(D)** Longitudinal section of a secondary spermatocyte showing a lengthened nucleus (n), the basal body of the flagellum (bb), an incipient acrosome (a), an electron-clear vacuole (v), and a cytoplasmic bridge (arrow) with a sister spermatocyte. **(E-F)** Longitudinal section of spermatids showing an ellipsoidal nucleus (n) with a peripheral indentation (id) and highly-packed chromatin, except for an electron-clear central area (ea). It is also shown a single, large mitochondrion (mi), an acrosome (a), an electron-clear vacuole (v), the basal body (bb) and the accessory centriole (ac) migrated to the cell side opposite the flagellum insertion.

was a choanocyte that recently left the chamber after engulfing the spermatozoon. The spermiocyst was membrane-bounded and consisted of a 2 x 1 μm, very electron-dense body with an electron-clear area (Figs 15 D-E) reminiscent of that seen in the condensed nucleus of spermatids (Figs 11F, 14A). However, no other organelle in addition to the nucleus was observed (see Discussion).

We failed to capture the moment of oocyte fertilization in any histological section, but noticed that upon fertilization a cellular follicle appeared to envelope the newly formed zygotes (Fig. 15F). We suspect that it formed rapidly from nurse cells trans-differentiating into flattened (0.2μm-thick), pseudo-epithelial cells, which joined each other through interdigitate junctions (not shown). Because the follicle located between the bacterial layer that surrounds the embryo and its outer envelope of collagen microfibrils (Fig. 15F), the latter structure became a sort of basement membrane for the newly formed follicular epithelium. The follicle enclosed embryos tightly during the pre-gastrular phase of embryogenesis, while an empty space was visible between it and the embryos after gastrulation (Fig. 2E). This suggests that postgastrular embryos

experienced some compaction to form the larva (Fig. 5). At no stage we observed cytoplasmic bridges connecting developing embryos and follicle cells.

During cleavage, the bacteria that surrounded the embryos spread into the cleavage furrows (Fig. 15F), reaching the intercellular spaces and ending among the cells of the embryo (Fig. 15G). By this peculiar process, which had also been described in other homosclerophorids (Ereskovsky and Boury-Esnault 2002), symbiotic bacteria that never entered the egg were directly transmitted to the internal cavity of the free-swimming larva.

Discussion

In most marine invertebrates, the phylum Porifera included, sexual reproduction tends to be confined to narrow thermal ranges (Kinne 1970). Studies on reproductive patterns in a variety of temperate Demosponges suggest that the seasonal rising of seawater temperature is the main cue triggering gametogenesis (e.g., Diaz 1973; Fell 1976b; Elvin 1976; Lepore et al. 2000; Usher et al. 2004; Mercurio et al. 2007). However, the gametogenesis of *Corticium candelabrum* does not fit this pattern. As its oogenesis was continuous, there was not an obvious onset associated with the rise of temperature. Furthermore, the rate of oocyte production was apparently stimulated by decreasing temperatures (Fig. 3). Similarly, spermatogenesis onset was coincidental with the coldest month of the year. Therefore, low or declining temperatures rather than water warming may participate in the activation/regulation of gametogenesis in this sponge.

We failed to capture in our histological sections the exact moment in which transformation of somatic into gonial cells took place. Nevertheless, indirect evidence suggested that oogonia derived from archaeocytes. Early oocytes and archaeocytes had similar positions in the mesohyl, together with similar size, morphology, and affinity for stains. Indirect, but stronger, evidence also indicated that spermatogonia, which were flagellated cells, derived from choanocytes. Transformation of entire choanocyte chambers (30 to 40 μm in diameter) into spermatic cysts (50-60 μm in average diameter) is postulated as the most probable mechanism. The small size of cysts suggested that neither choanocyte chambers fuse to make a cyst (Simpson 1984) nor

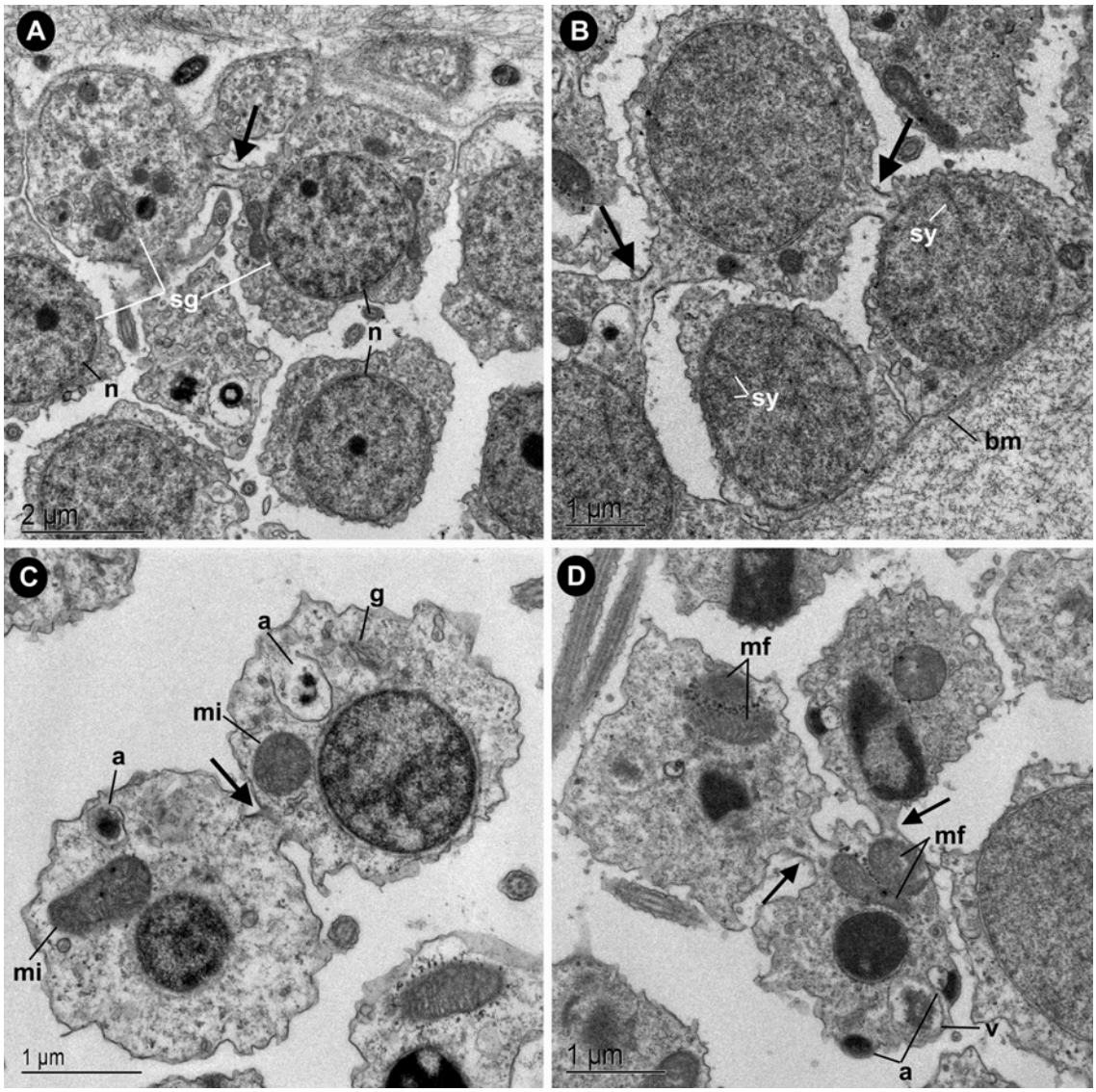

Figure 12. Cytoplasmic bridging in the spermatogenesis. **(A)** Bridge (arrow) between 2 spermatogonia in the peripheral stratum of the cyst. Note the nucleolate nucleus (n) and the bi-layered structure of the spermatogonial stratum (sg). **(B)** Detail of bridges (arrows) between different layers of primary spermatocytes adjacent to the basement membrane (bm). The synaptonemal complexes (sy) within the nuclei indicate that all spermatogonia have become primary spermatocytes. **(C)** Bridge (arrow) between secondary spermatocytes, which show a mitochondrion (mi), a developing acrosome (a), and the Golgi apparatus (g). **(D)** Bridges (arrows) connecting sister spermatids. Note the process of mitochondrial fusion (mf), the electron-clear vacuole (v), and the C-shaped acrosome, represented by 2 acrosomal vesicles) (a).

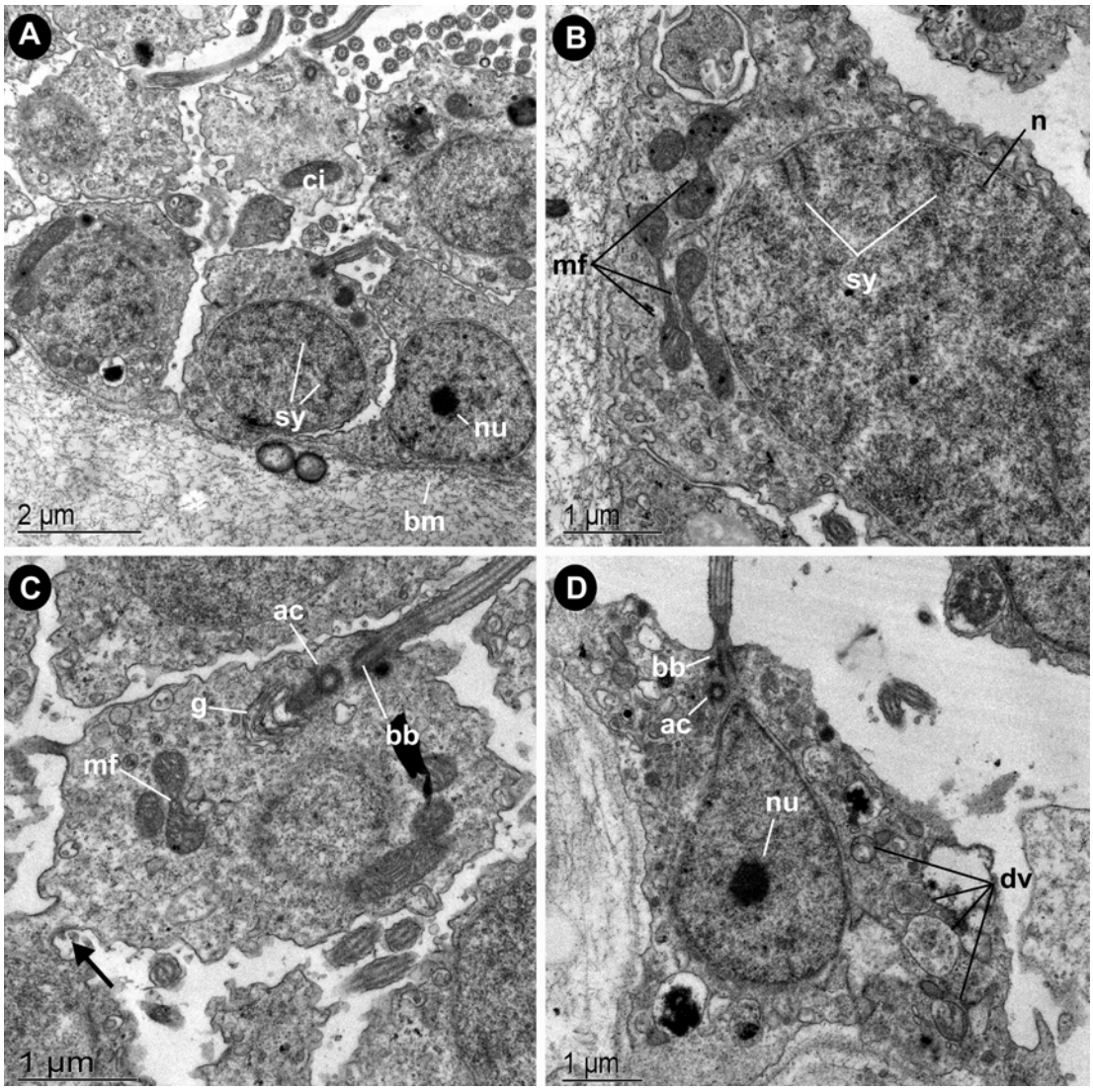

Figure 13. Spermatogonia and primary spermatocytes vs choanocytes. **(A)** Peripheral stratum of a spermatic cyst made of spermatogonia and primary spermatocytes. Note the occurrence of a flagellum (ci) and a nucleolus (nu) within the nuclei of a spermatogonium, the synaptonemal complexes (sy) within the nuclei of primary spermatocytes, and the basement membrane of the cyst (bm). **(B)** Primary spermatocyte showing fusing mitochondria (mf) and synaptonemal complexes (sy) in the nucleus (n). **(C)** Primary spermatocyte showing mitochondrial (mi) fusion, a well-developed Golgi apparatus (g) close to the accessory centriole (ac), the basal body of the flagellum (bb), and a cytoplasmic bridge (arrow). **(D)** Longitudinal section of a choanocyte showing the oval nucleolate (nu) nucleus, several digestive vacuoles (dv), the basal body (bb), and the accessory centriole (ac) of the flagellum.

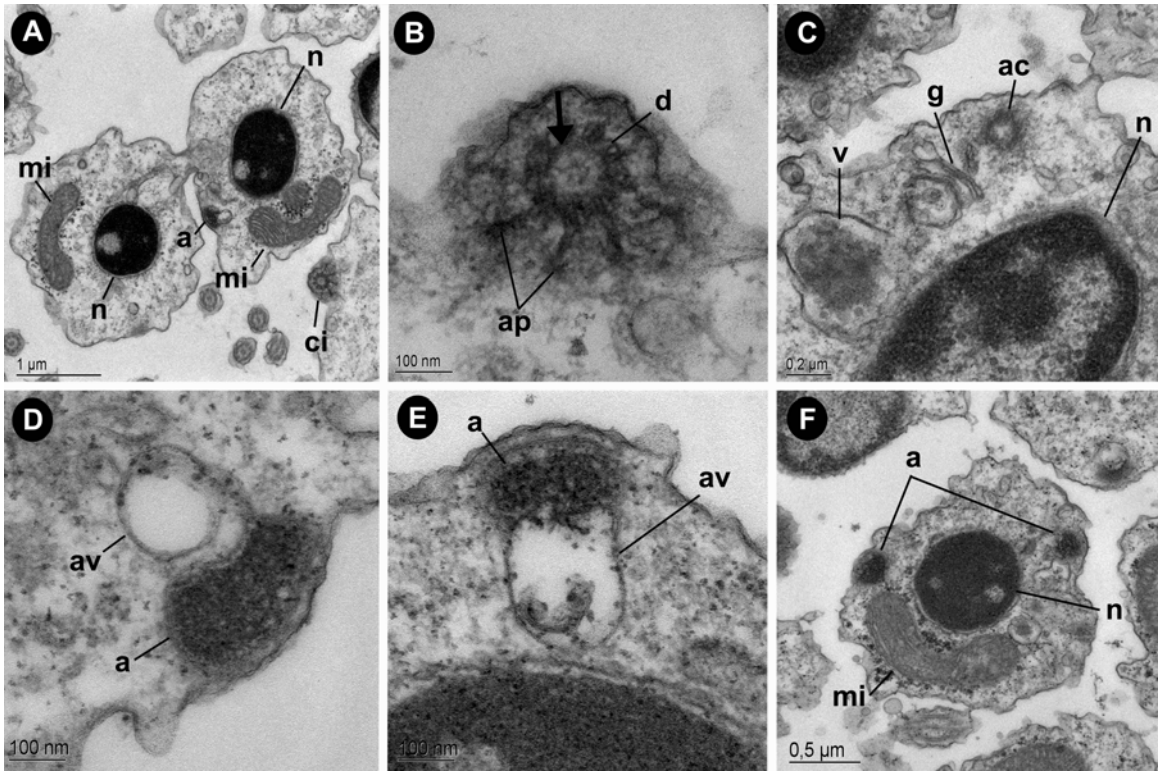

Figure 14. Special features at different spermatogenesis stages. **(A)** Spermatids connected by cytoplasmic bridges (arrows). Note the highly-compacted chromatin in both nuclei (n), the occurrence of a single mitochondrion (mi), and the presence of the acrosome (a). Additionally, on the right side of the micrograph, a flagellum insertion (ci) sectioned at the transition zone is seen. **(B)** Magnification of the flagellum transition zone seen in Fig. 14A, showing microtubule doublets connected to the anchoring points (ap) by the alar sheets. **(C)** Secondary spermatocyte showing the Golgi apparatus (g), a vacuole -probably derived from Golgi cisternae- with electron-dense content (v), the accessory centriole (ac), and the semi-condensed nucleus (n). **(D-E)** Formation of the acrosome (a) in the spermatid. Note the electron-clear vacuole (av) below a growing acrosome (a) of granular electron-dense content. **(F)** Spermatid showing a very electron-dense nucleus (n), a large mitochondrion (mi), and the two vesicles of a C-shaped acrosome (a).

choanocytes multiply by mitosis prior to cyst formation (Shore 1971). The transformation of choanocytes into spermatogonia involved loss of the collar but maintenance of nucleolus, as known in other sponges (e.g., Diaz and Connes 1980; Simpson 1984).

Figure 15. Sperm uptake, spermiocyst and intercellular transmission of bacteria to embryos. **(A)** Spermatozoon (sz) entering a choanocyte (ch) chamber. **(B)** Enlarged view of the free-swimming spermatozoon framed in Fig 15A, showing the nucleus (n), the mitochondrion (mi), and the basal body (bb) of the flagellum. **(C)** General view of a choanocyte chamber (ch), in which a choanocyte containing a putative spermiocyst (sk) left the chamber to become a carrier cell. **(D)** Magnification of the carrier cell showing a spermiocyst in its cytoplasm (sk), a large electron-clear digestive vacuole (dv), and a large nucleus (n). **(E)** Detail of the membrane-bounded (mb) spermiocyst (sk). Note the highly-condensed chromatin in the nucleus (n) and the electron-clear central area of it (arrow). **(F)** Symbiotic bacteria (ib) entering the intercellular space between two cells of an early-stage developing embryo. Note the nucleus (n) of the follicular cell (fc) enveloping the embryo. **(G)** Bacteria (ib) inside the cleavage furrow of an embryo.

We found cytoplasmic bridges between spermatogonia suggesting spermatogonial mitosis before differentiation into primary spermatocytes, a feature only observed in few sponges to date, but already known in other homosclerophorids (Tuzet and Paris 1964; Diaz and Connes 1980; Gaino et al. 1986b).

Unlike in many other demosponges, gamete production and brooding in *C. candelabrum* caused no obvious disruption of the general pattern of choanocyte chambers. A possible explanation could be the low tissue occupancy by gametes in *C. candelabrum*, which was about 3% for oocytes and about 1% for spermatic cysts. Nevertheless, this may not be a relevant reason, since low occupancy by oocytes has also been reported in several other demosponges – 6% in *Tethya citrina* and 2% in *Tethya aurantium* (Corriero, Sarà and Vaccaro 1996); 2.3% in *Mycale* sp. and 1% in *Verongia gigantea* (Reiswig 1973); less than 1% in *Aplysina cauliformis* (Tsurumi and Reiswig 1997), and only some of them experience mesohyl disruption. Tissue occupancy by spermatic cysts in *C. candelabrum* was identical to that reported for *Ircinia strobilina* (Hoppe 1988) and only slightly smaller than the 5% to 10% recorded in *Mycale* sp. (Reiswig 1973). Nevertheless, the occupancy values in these 3 species, which are characterized by internal fertilization and viviparism, are low when compared to 50% occupancy by cysts in *Aplysina cauliformis* (Tsurumi and Reiswig 1997), which is an externally-fertilizing species.

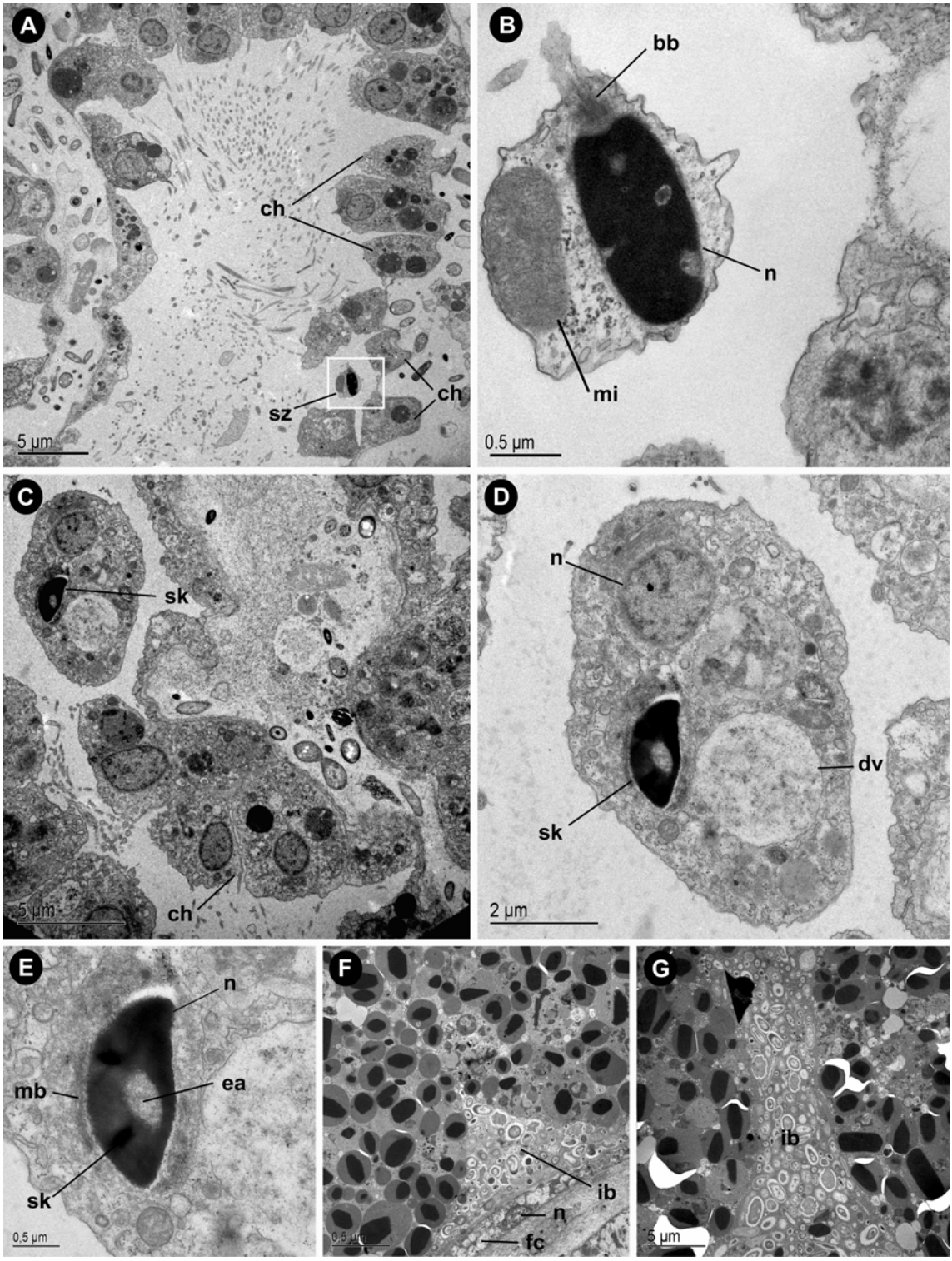
A
ch
ch
sz
ch
5 µm
B
bb
n
mi
0.5 µm
C
sk
ch
5 µm
D
n
dv
sk
2 µm
E
n
mb
ea
sk
0,5 µm
F
ib
n
fc
0,5 µm
G
ib
5 µm

Like gametes, embryos took no much mesohyl space (up to a maximum of 7.7%), a trait that may help to preserve global tissue functionality during the brooding process. Interestingly, once pregastrular embryos gastrulated, they stopped increasing in size, experiencing just cell reorganizations. We also noticed that mean size of post-gastrular embryos tended to decrease over time, with embryos produced towards the end of the reproductive period (mid July to August) being progressively smaller than those produced in June (Fig. 5). This pattern may result from gradual depletion of maternal reserves and endosymbiotic bacteria that will be transferred to late oocytes and embryos. Such a size dynamics suggested that seawater temperature, which was substantially high at the time of late embryogenesis, did not appear to have an appreciable impact on the growth of late-stage embryos. On the other hand, we cannot discard that the predictable temperature rising during spring could help to synchronize development of pregastrular embryos, and, if so, incidentally larval release. A temperature-controlled larval release has been suggested for other demosponges (e.g., Zea 1993; Maldonado and Young 1996; Mariani et al. 2000), though never proved experimentally.

Some aspects of gametogenesis dynamics in *C. candelabrum* are noteworthy. According to our observations, oocyte growth in *C. candelabrum* took about 7 to 8 months, being among the longest ones recorded in the phylum Porifera. A long oogenesis has been reported for other demosponges, such as *Cliona celata* and *Haliclona oculata* (Wapstra and van Soest 1987), *Halichondria okadai* (Tanaka-Ichiara and Watanabe 1990), *Halichondria panicea* (Witte et al. 1994) and *Halisarca nahatensis* (Chen 1976). The physiological and ecological reasons for extended oogenesis are poorly understood. In the case of *C. candelabrum*, a possible cause could be that most yolk appeared to be self-synthesized by the oocyte. In other sponges, such as for instance those in the genus *Chondrilla*, a substantial amount of yolk is synthesized by nurse cells and transferred to the oocytes (e.g., Maldonado et al. 2005). Oogenesis is completed in just 34 days in the only *Chondrill*a species studied in detail (Fromont 1999), which suggests that contribution by nurse cells substantially shortens oocyte development. In contrast, a large portion of the yolk in *C. candelabrum* may derive from phagocytosis of the endosymbiotic bacteria that accumulated around the oocytes. We assume that all bacteria engulfed by early and late-stage oocytes were

digested, since only intercellular symbiotic bacteria occurred in the larva (not shown), being those squeezed through the cleavage furrows of pre-gastrular embryos. It is unclear whether the bacterial accumulations around the oocytes resulted from 1) migration (chemotaxis?) of intercellular bacteria to proliferate in the vicinity of oocytes, 2) exocytosis of bacteria transported by nurse cells, or 3) the combined action of both processes. A substantial contribution by nurse cells to these accumulations is more likely, because massive events of neither bacterial migration nor bacterial division were noticed. Other plausible reason for an extended oogenesis in *C. candelabrum* is that, by using oocytes that slowly grow during winter, this sponge avoids the peak of intense food competition in the Mediterranean spring. At that time most other sublittoral sponges are assumed to ingest large amounts of bacteria to generate the yolk demanded by their seasonal reproductive activity.

If the reasons why *C. candelabrum* experiences extended oocyte growth remain unclear, the situation does not get any better when attempting to understand why a continuous oogenesis is required to produce embryos during only a brief period of the year. Although temperature has no apparent relationship with the onset of gametogenesis, we cannot discard its role in accelerating growth rates of the new oocytes appeared 2 or 3 months before the earliest spermatic cysts, synchronizing their maturation with that of slowly-developing oocytes occurring in the mesohyl several months in advance. Nonetheless, we found that about 40% of oocytes were still immature (according to their size) at the time of sperm release. The fate of such oocytes remains unclear, though we detected their progressive disappearance from the tissues (Fig. 4). They may be reabsorbed, as known in some calcareous sponges (Dubosq and Tuzet 1937; Colussi 1958) and many demosponges (Gilbert 1974; Gallissian and Vacelet 1976; Tanaka-Ichihara and Watanabe 1990; Fell 1969). Additionally, they could also be ingested by late-stage oocytes (e.g., Maldonado et al. 2005) and early embryos (e.g., Sarà 1955), benefiting their maturation. This oocyte cannibalism is known in many invertebrates (Zihler 1972; Bierne and Rué 1979; Beams and Kessel 1983).

Very few demosponges other than *C. candelabrum* produce new oocytes over many months of the year, though some follow this pattern, such as *Haliclona ecbasis* (Fell 1974), *Hippiospongia lachne* (Storr 1964), *Halisarca dujardini* (Lévi 1956), and

Mycale contarenii (Corriero et al. 1998). Yet the case of *C. candelabrum* is distinct because new oocytes are produced every month of the year. It means that oocytes appeared not only at the time in which growing embryos occurred in the mesohyl and there was no available sperm, but also immediately after larval release, without allowing the period of post-reproductive recovery reported for other demosponges (e.g., Fell 1974; Chen 1976; Turón et al. 1999). Continuous production of oocytes should not be confused with oocytes occurring in the mesohyl for long periods as the result of 2 or more cycles of oocyte production (cohorts) over the year, as found in some calcareans (Duboscq and Tuzet 1937; Tuzet 1964; Vacelet 1964) and several demosponges (Lévi 1951, 1956; Sarà 1961; Fell 1969).

Spermatogenesis in *C. candelabrum*, which extended for about 4 to 5 months at the population level, is a relatively short process when compared with oogenesis. However, it is relatively long when compared with spermatogenesis in other demosponges, which usually lasts from 1 to few weeks (e.g., Reiswig 1983; Boury-Esnault and Jamieson 1999). We detected spermatic cysts in *C. candelabrum* from mid March to late July (Fig. 1, 3). Nevertheless, it is likely that some cysts first appeared in February, right after our monthly sampling. Occurrence of some undetected spermatic cysts in February is supported by appearance of some early embryos in March (Fig. 1, 3). Spermatozoon differentiation within a cyst was estimated to be completed in about a couple of weeks. Notwithstanding, extended production of new cysts by the individuals makes the sponge population to be engaged in sperm production for several months. During summer sampling, we found that some of the non-tagged individuals still contained spermatic cysts in July, while all 5 tagged individuals finished spermatogenesis one month in advance. Therefore, spermatogenesis was asynchronous at not only the individual level but also the population level. Extended spermatogenesis at the population level may increase the chances of fertilization, because mature oocytes were available over several months. A relatively asynchronous spermatogenesis has been reported in other homosclerophorids (Gaino et al. 1986b), as well as in several halisarcid demosponges (Lévi 1956; Chen 1976) and the astrophorid *Geodia cydonium* (Mercurio et al. 2007).

Not only is the dynamics of spermatogenesis in this sponge peculiar when compared with most other demosponges, but also some cytological aspects of its

spermatic cysts. They lack a cellular follicle, a condition never found in other demosponges (Boury-Esnault and Jamieson 1999), except for other homosclerophorid species (Gaino et al. 1986b). Interestingly, though spermatogenesis and cyst structure in *C. candelabrum* are relatively similar to those known in higher invertebrates (e.g., Alberts et al. 1993), the origin of its spermatogonial cells -from trans-differentiated somatic cells- strongly departs from the general model found in most animals. We also found that the spermatozoon flagellum was provided with alar sheets and anchoring points (Figs 14A-B), as in the remaining Metazoa. To date, such structures were thought to occur only in the sperm of Eumetazoa but not in that of the Porifera (Franzén 1996).

Most aspects of the events that take place between sperm release and fertilization remain little documented in Demospongiae. Unfortunately, we failed to document any event of sperm release despite increasing sampling effort. Nonetheless, we found swimming spermatozoa within the choanocyte chambers (Fig. 15A-B). Besides, we found a putative spermiocyst being transported by a carrier cell (Fig. 15C-E). While spermiocysts have been described by electron microscopy in several calcareous sponges (e.g., Nakamura et al. 1998), they have not been studied by TEM in any demosponge to date. The putative spermiocyst documented herein, which consisted of a highly condensed nucleus only, strongly differed in its general organization from those known in the class Calcarea, in which various organelles, such as the acrosome, mitochondria, and part of the axoneme, are evident until the carrier cell contacts the oocyte (e.g., Nakamura et al. 1998).

The histological monitoring suggested that the success of internal fertilization in this sponge was close to 100%. Information on fertilization success in sponges is only available for *Xestospongia bergquistia* (Fromont and Bergquist 1994), finding a value close to 70%. Much lower average values (20%) have being estimated for various sessile marine organisms with external fertilization (Levitan 1995). Like *C. candelabrum*, some corals are sperm casters that is, releasing sperm to the water column but experiencing internal fertilization of oocytes. However, the available data for these organisms indicate that only about 10% of oocytes are finally released as larvae (e.g., Brazeau and Lasker 1992). Because mature sperm cysts and mature oocytes located in the mesohyl of *C. candelabrum* just a few microns away from each other (Fig. 2), mechanisms to prevent accidental self-fertilization should occur. Though the possibility

of self-fertilization in sponges has never been examined experimentally and cannot be ruled out, self-fertilization incidence, if any, is expected to be extremely low, as in corals. Special mechanisms minimizing self-fertilization, such as delayed emission of polar bodies and capability for self-recognition of gametes, have been postulated in corals (Babcock 1986; Harrison and Wallace 1978).

In summary, the features of the reproductive process of *C. candelabrum* are largely consistent with those observed in other homosclerophorids, but depart in several aspects from the process known in most other demosponges, contributing to support the emerging idea that the homosclerophorids are a distinctive group within the class Demospongiae.